Tetrahedron 72 (2016) 464–471

Contents lists available at ScienceDirect

Tetrahedron

journal homepage: www.elsevier.com/locate/tet

Difluoroboron complexes of functionalized dehydroacetic acid: electrochemical and luminescent properties

Samira Baaziz [a,b], Nathalie Bellec [a,*], Yann Le Gal [a], Rachedine Kaoua [a,b,c], Franck Camerel [a], Saleha Bakhta [a,b], Bellara Nedjar-Kolli [b], Thierry Roisnel [a], Vincent Dorcet [a], Olivier Jeannin [a], Dominique Lorcy [a]

[a] Institut des Sciences Chimiques de Rennes (ISCR), UMR 6226 CNRS-Université de Rennes 1, Campus de Beaulieu, 263 avenue du Général Leclerc, Bat 10A, 35042 Rennes Cedex, France
[b] Laboratoire de Chimie Organique et Appliquée, Université des Sciences et de la Technologie Houari Boumediene (USTHB), 16111 Alger, Algeria
[c] Institut des Sciences, Université Mohamed Akli Ouelhadj, 10000, Bouira, Algeria

ARTICLE INFO

Article history:
Received 6 October 2015
Received in revised form 16 November 2015
Accepted 17 November 2015
Available online 26 November 2015

Keywords:
Dehydroacetic acid
Tetrathiafulvalene
Ferrocene
Boron difluoride complex

ABSTRACT

A series of dehydroacetic acid difluoroboron complexes functionalized by a phenyl ring or an electroactive core (tetrathiafulvalene or ferrocene) were synthesized and characterized. The redox properties of these derivatives have been analyzed by cyclic voltammetry and the molecular structures of some of the difluoroboron complexes are presented and discussed. The photophysical properties of selected difluoroboron complexes were determined in solution and in the solid state evidencing an AIEE (Aggregation Induced Enhancement Emission) phenomenon.

1. Introduction

Dehydroacetic acid (DHA) has mainly been investigated as precursor of various heterocyclic compounds of potential biological interest.[1] In addition due to its planar structure, its reactivity and also its ability to act as a chelating ligand, this synthon could be used as a coordinating part in precursor of molecular materials based on tetrathiafulvalene (TTF) for example.[2] Indeed, DHA and the Schiff base of DHA exhibit similar binding sites as the well-known acetylacetonate group (acac) and thus can complex numerous metallic ions.[3,4] Besides metallic ions, DHA and its Schiff base can also complex difluoroboron moiety (Chart 1). The formation of such difluoroboron complexes present two advantages: (i) it enhances the reactivity of DHA itself and (ii) some of these derivatives can exhibit fluorescence properties.[5]

Our current interest in the synthesis of various electroactive ligands containing the TTF core for the elaboration of molecular materials,[6] prompted us to investigate the possibility to graft, on the DHA, this electroactive moiety. The TTF[7] is not the only electrophore, which exhibits easily accessible and reversible oxidation processes, indeed the ferrocene (Fc)[8] is also easily oxidized to the ferrocenium ion. We reported the synthesis of a TTF functionalized by a DHA-BF_2 moiety where the fluorophore and the electrophore were connected thanks to the reaction of TTF-hydrazone with DHA.[9]

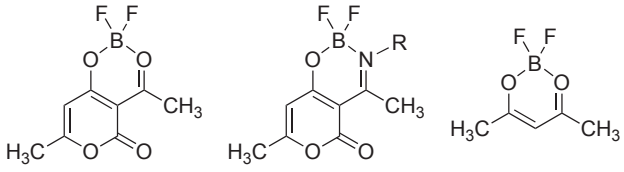

Chart 1. Binding sites of DHA, Schiff Base of DHA and acacH molecules.

Herein we investigated the synthesis of DHA-BF_2 and Schiff base of DHA-BF_2 functionalized either by an electrophore, the TTF and the Fc, or by a phenyl group in order to analyse the influence of the electrophore on the fluorophore properties. For that purpose, three approaches were used: i) Wittig reaction at the 6 position involving the aldehydes bearing an electroactive unit and a phosphonium salt of DHA, ii) condensation reactions of these aldehydes with DHA-

* Corresponding author. Fax: +33 2 23 23 67 38; e-mail address: nathalie.bellec@univ-rennes1.fr (N. Bellec).

http://dx.doi.org/10.1016/j.tet.2015.11.034
0040-4020/

BF_2 at the acetyl position and iii) condensation of the aldehydes on the DHA-hydrazone. Three different aldehydes were used, two with an electroactive unit (Fc and TTF) and one, which could serve as a reference: benzaldehyde. Depending on the reaction used, the spacer group between the DHA moiety and the electroactive part will be different as well as the position of the connecting part on the DHA core (Chart 2).

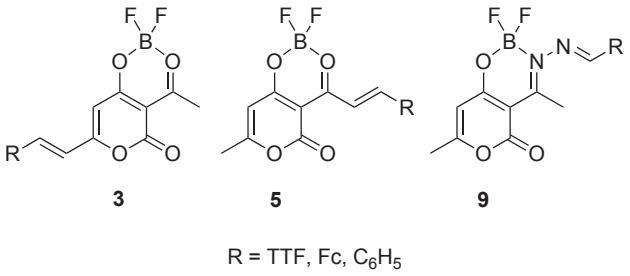

Chart 2. Target complexes.

2. Results and discussion

Wittig olefination starting from triphenylphosphonium salt **1** enabled us to introduce the electroactive moiety on the methyl group at the 6 position of DHA.[10] The addition of 2 equiv of sodium methoxide to salt **1** generates the corresponding ylide, which reacts with ferrocenecarboxaldehyde (Fc-CHO), trimethyltetrathia fulvalene carboxaldehyde (Me_3TTF-CHO) and benzaldehyde to afford compounds **2a, 2b** and **2c**[10] in 22%, 57% and 48% yield, respectively (Scheme 1). The addition of an excess of $Et_2O{\cdot}BF_3$ to a toluene solution of **2a**–**c** under inert atmosphere afforded the corresponding difluoroboron complexes **3a**–**c** in very good yields as colored solids. Purification cannot be performed by column chromatography as a large amount of these complexes **3a**–**c** get stuck on silica. The other part, which was eluted correspond to the starting material **2a**–**c** indicating that upon chromatography, these difluoroboron complexes undergo decomplexation. Moreover, compounds **2b** and **3b** are poorly soluble in usual organic solvents. The ^{1}H NMR spectra of these derivatives **2a**–**c** and **3a**–**c** exhibit two doublet signals associated with the protons of the formed ethylenic bridge with a coupling constant of 15–17 Hz, which indicate a *trans* coupling across the double bond.[11] Disappearance of the hydroxyl signal (δ=16.6 ppm) confirms the formation of complexes **3**.

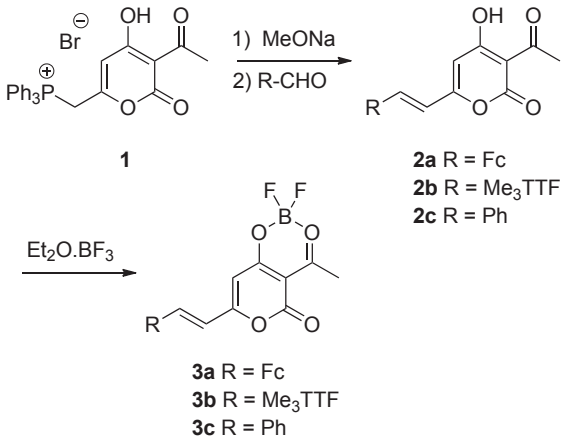

Scheme 1. Synthesis of complexes **3a**–**c**.

The second strategy that we studied in order to graft an electroactive core to a DHA-difluoroboron complex consists in the use of 3-acetyl-6-methyl-2-oxo-*2H*-pyran-4-yl difluoroborate **4** as starting material. Indeed, DHA-difluoroboron complex **4** in the presence of various aldehydes in acetic anhydride medium is known to give condensation compound at the acetyl position.[12] Moreover, compared with DHA itself the reactivity of the methyl group of the acetyl moiety is considerably increased by the presence of the boron difluoride complex. Thus, we prepared the complex **4** through the reaction of boron trifluoride diethyl etherate with dehydroacetic acid.[12] Then by heating the aldehydes, Fc-CHO, Me_3TTF-CHO or benzaldehyde with complex **4** in acetic anhydride, we formed the targeted complexes **5a**–**c** as green solids, in 60% yield for **5a** but in lower yields for **5b**–**c**, 7 and 12%, respectively (Scheme 2). This difference in the yields can be easily explained by the different work up used to obtain these complexes. Indeed, **5a** precipitated in the medium while for **5b** and **5c** purification by column chromatography was performed and as already mentioned for **3a**–**c**, upon purification by column chromatography decomplexation of **5b**–**c** partially occur. On the other hand, it is also possible to form the corresponding uncomplexed derivatives **6a**–**b** in good yields (64–75%) through the hydrolysis of **5a**–**b** in ethanol in the presence of Na_2CO_3.[12] Here again, analyses of the ^{1}H NMR spectra indicate that the ethylenic bridge formed is under the *trans* configuration as a typical $^3J_{trans}$ coupling constant of 15–16 Hz is observed. The influence of the electron donating ability of the *R* group can also be observed on these spectra as the chemical shift observed for these ethylenic protons is downfield for the benzene derivatives compared with the one bearing an Fc or a TTF core.

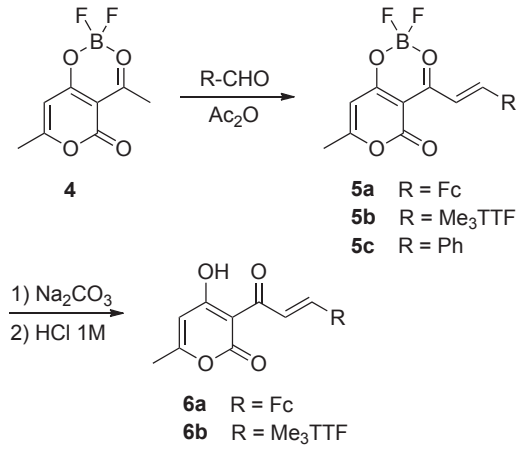

Scheme 2. Synthesis of complexes **5a**–**c**.

Crystals suitable for X-ray diffraction studies have been obtained for compounds **5a** and **5b** by slow concentration of a dichloromethane solution. The molecular structures of **5a** and **5b** are represented in Fig. 1 and selected bond lengths and bond angles are collected in Table 1. The DHA-boron moieties in compounds **5a** and **5b** exhibit similar trends: an overall flat geometry with the boron out of the plane with the six-membered difluoroboron ring folded along the O···O axis with an angle of 20.8° and 17.3° for complexes **5a** and **5b**. Within both structures, the DHA boron moiety is connected to the electroactive part with a C=C bond under a *trans* configuration. The geometry of the TTF in complex **5b** is almost planar as the folding angles along the S···S axis are only 0.04 and 2.82°. The bond lengths of the TTF core are those expected for a neutral TTF (central C=C of 1.346 (6) Å).

For the preparation of the target derivatives through the third approach, we prepared DHA-hydrazone **7** according to literature procedure by adding 1 equiv of hydrazine monohydrate to an ethanolic solution of DHA.[13] The condensation reaction occurs immediately and an abundant precipitate appears in the media at room temperature to give the corresponding hydrazone **7**. Crystals

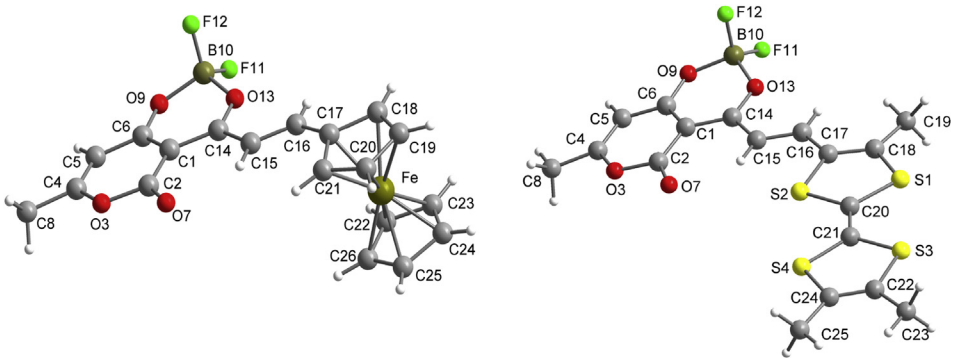

Fig. 1. Molecular structure of **5a** (left), **5b** (right).

suitable for an X-ray diffraction study were obtained for **7** and the molecular structure is shown in Fig. 2. DHA-hydrazone **7** exhibits a planar geometry with the establishment of intramolecular hydrogen bonding between the O–H and the sp^2 N atom of the hydrazone (1.821 (1) Å) forming a pseudo six membered cycle.

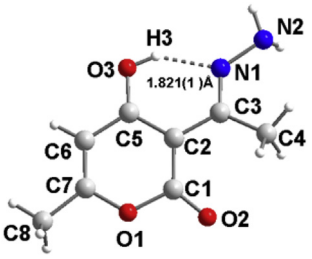

Fig. 2. Molecular structure of DHA-hydrazone **7**.

Table 1
Comparison of selected bond lengths in Å and angles in ° of the chelate ring in complexes **5a** and **5b**

Bond lengths	5a	5b	Bond angles	5a	5b
C15–C16	1.350 (4)	1.352 (5)	C14–C15–C16	122.5 (3)	121.4 (3)
C14–C15	1.425 (3)	1.425 (5)	O13–C14–O15	116.7 (2)	117.1 (3)
C14–O13	1.304 (3)	1.302 (4)	O13–C14–C1	118.7 (2)	118.9 (3)
C1–C14	1.440 (4)	1.421 (5)	C14–C1–C6	118.8 (2)	119.2 (3)
C1–C6	1.397 (3)	1.414 (5)	C1–C6–O9	122.2 (2)	121.9 (3)
C6–O9	1.305 (3)	1.303 (4)	C6–O9–B10	121.2 (2)	121.3 (3)
O9–B10	1.483 (4)	1.503 (5)	O9–B10–O13	110.5 (2)	110.6 (3)
B10–O13	1.481 (3)	1.476 (5)	B10–O13–C14	123.5 (2)	124.3 (3)

Reactions were carried out between DHA-hydrazone **7** and the three aldehydes (Fc-CHO, Me_3TTF-CHO and benzaldehyde). These reactions, with the electroactive moieties were performed in THF in the presence of HCl to afford **8a** and **8b** in 74% and 53% yield, respectively as dark colored solids (Scheme 3).[9] The reaction of DHA-hydrazone **7** with benzaldehyde was carried out in refluxing EtOH and led to the desired derivative **8c** in 75% yield. In order to prepare the difluoroboron complex of the derivatives **8a**–**c**, we added an excess of $Et_2O{\cdot}BF_3$, in the presence of triethylamine, to a solution of **8a**–**c** in dichloromethane under inert atmosphere. The difluoroborane complexes **9a**–**c** were isolated after purification by column chromatography. It is worth noting that in this case decomplexation upon column chromatography was not observed.

Crystals suitable for X-ray diffraction studies have been obtained for compounds **8a** and **9a** and their molecular structures are represented in Fig. 3. Within compound **8a**, analysis of the bond lengths of the linker between the DHA and the ferrocene moieties together with the finding of a hydrogen atom on N13, which was introduced in the structural model through Fourier difference maps analysis, indicate that the linker is not an azino structure but a hydrazone one. It is worth noting that for the starting material, DHA-hydrazone, the crystal structure determination led to the other tautomer, the imine form. Actually it is known that, imine-enamine tautomerism of pyronic derivatives such as DHA exists. Moreover, depending on the substituent, either the enamine or the imine's form is favored (Scheme 4).[14] Herein, the enamino ketone form for **8a** is obtained. Intramolecular hydrogen bonding is observed between the N–H and the O atom within this structure leading to a six-membered cycle. Except for the ferrocenyl group the molecule **8a** exhibits a planar skeleton.

Besides the orientation of the ferrocenyl group with regard to the DHA moiety the molecular shape of the difluoroboron complex **9a** is very similar to the one of the starting ligand **8a**. Indeed the ferrocenyl groups are pointing in opposite direction. Variations can also be noticed on the bond lengths and bond angles mainly on the chelate ring. Selected bond lengths and angles of the chelate rings are collected in Table 2. Within the complex **9a**, the C16–C21 bond is shortened compared to ligand **8a** (ca. 0.05 Å) while the C21–O24 bond is lengthened (ca. 0.04 Å). Due to the presence of the difluoroboron moiety, the bond angles of the chelating moiety are different. Otherwise, in complex **9a**, the chelate ring is less distorted than complexes **2a** and **2b** as the torsion angle is only 7.19 (24)°.

Table 2
Comparison of selected bond lengths in Å and angles in ° of the chelate ring in ligand **8a** and complex **9a**

Bond lengths	7	8a	9a	Bond angles	7	8a	9a
C11–N12		1.288 (2)	1.285 (5)	C10–C11–N12		122.99 (14)	117.1 (3)
N12–N13	1.416 (2)	1.3918 (17)	1.417 (4)	C11–N12–N13		111.88 (12)	117.6 (3)
N13–C14	1.312 (2)	1.3225 (19)	1.331 (5)	N12–N13–C14	122.78 (15)	123.40 (13)	113.1 (3)
C14–C16	1.442 (2)	1.432 (2)	1.440 (5)	N13–C14–C16	117.71 (15)	116.40 (13)	117.4 (4)
C16–C21	1.444 (2)	1.442 (2)	1.388 (6)	C14–C16–C21	121.01 (14)	121.11 (13)	120.1 (4)
C21–O24	1.266 (2)	1.2645 (18)	1.305 (4)	C16–C21–O24	123.14 (15)	123.36 (13)	123.2 (3)
O24–B25		—	1.465 (5)	C21–O24–B25		—	124.6 (3)
B25–N13		—	1.572 (6)	O24–B25–N13		—	108.8 (3)
				B25–N13–C14		—	125.1 (3)

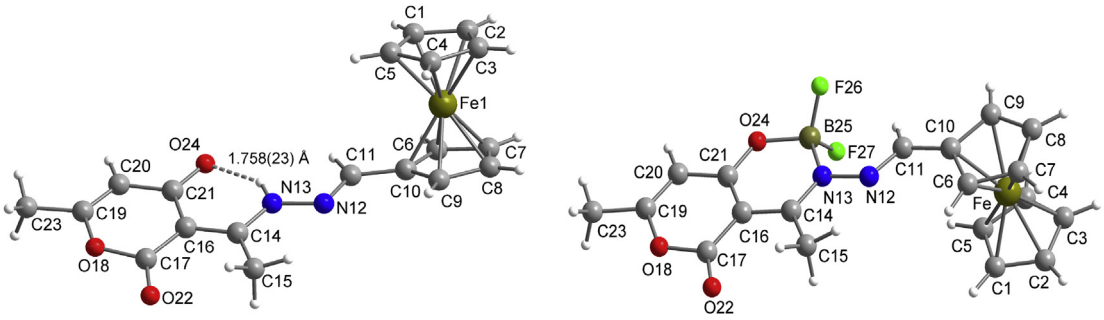

Fig. 3. Molecular structure of **8a** (left) and **9a** (right).

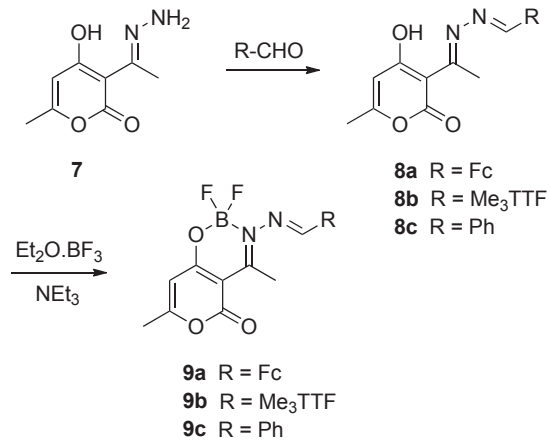

Scheme 3. Synthesis of complexes **9a**–**c**.

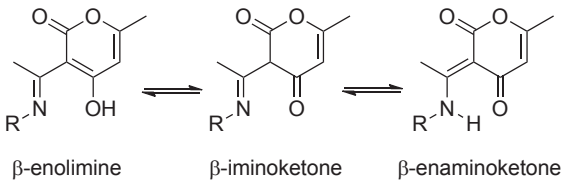

Scheme 4. Imine-enamine tautomerism.

In order to study the influence of the complexation on the donating ability of the electroactive moieties, we performed electrochemical investigations on the starting ligands and on the difluoroboron complexes. For all the ferrocene derivatives one reversible monoelectronic wave is observed corresponding to the oxidation of the ferrocene moiety into the ferrocenium species. For all the TTF derivatives, two reversible monoelectronic oxidation waves are observed corresponding to the formation of the radical cation and the dication species, respectively. In both series, the TTF and the ferrocene, the presence of the boron complex induces a shift of the oxidation potentials towards more positive potentials indicating the electron withdrawing effect of the complexation with boron difluoride (Table 3). Similar effect has been observed previously on TTF-acetylacetonate complexes of difluoroboron.[15]

Absorption and emission spectra of selected compounds have been recorded in dichloromethane solutions and the data are gathered in Table 4. Absorption spectra of compound **4** display a strong absorption band centered at 327 nm together with a weaker one at 258 nm (Fig. 4). These absorption bands are attributed to n–π* and π–π* transitions centered on the DHA-BF_2 core. Interestingly, this compound was found to be highly

Table 3
Redox potentials $E_{1/2}$, CH_2Cl_2, Pt, SCE, $TBAPF_6$ 0.1 M, 100 mV^{-1}

Ligands	$E^1_{1/2}$	$E^2_{1/2}$	Complexes	$E^1_{1/2}$	$E^2_{1/2}$
2a	0.58		**3a**	0.63	
2b	0.37	0.85	**3b**	0.45	0.91
6a	0.61		**5a**	0.74	
6b	0.41	0.90	**5b**	0.48	0.94
8a	0.64		**9a**	0.67	
8b	0.38	0.87	**9b**	0.43	0.94

Table 4
Optical data measured in dichloromethane solution at 298 K

Compounds	λ_{abs}[a] (nm)	ε[a] ($M^{-1}.cm^{-1}$)	λ_F (nm)	$\Phi_{solution}$[b]
2a	534	5500	—	—
	387	20,800		
2b	567	10,000	—	—
	378	32,000		
	330	18,000		
	292	17,000		
3a	606	3500	—	—
	420	11,000		
	307	1800		
3b	636	7500	—	—
	410	16,200		
	385	16,900		
3c	395	39,000	—	—
4	327	26,000	360	0.745
	258	6000		
5a	645	14,500	358	0.007
	419	57,500		
	330	12,500		
5b	799	78,000	—	—
	432	26,000		
	324	14,000		
5c	406	40,000	450	0.004
	339	11,500		
6a	550	7500	—	—
	365	32,500		
6b	600	8200	—	—
	368	32,600		
8a	483	22,000	—	—
	376	122,000		
	361	133,000		
	248	86,000		
8b	525	6600	—	—
	383	36,300		
	369	34,400		
8c	379	35,000	—	—
	365	39,000		
9a	500	19,000	—	—
	353	111,000		
	289	45,000		
9b	558	6700	—	—
	369	34,000		
9c	358	26,500	440	0.002
Fc-CHO	460	6050	—	—
	338	14,000		
	268	69,700		

[a] $c \sim 10^{-5}$ M.
[b] Reference quinine sulfate (ϕ_{ref}=0.546 in H_2SO_4 1N).[16]

luminescent in solution under irradiation at 327 nm. An emission band centered at 360 nm extending from 330 nm to 450 nm in the visible region has been observed and a high fluorescence quantum yield around 74.5% has been determined relatively to quinine sulfate. The excitation spectra perfectly match absorption spectra, which is in line with a unique excited state and the weak Stokes' shifts (33 nm) observed is in good agreement with a singlet emitting state.

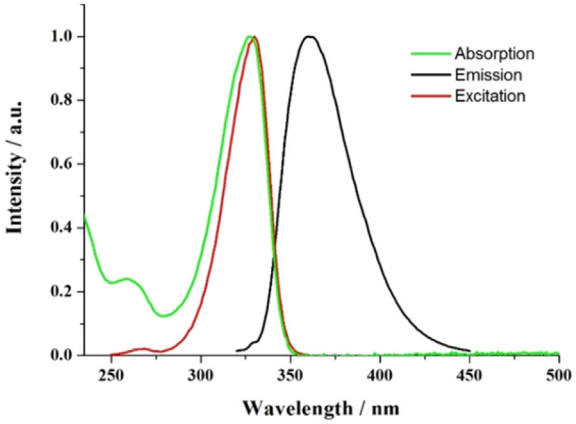

Fig. 4. Absorption, emission (λ_{ex}=300 nm) and excitation (λ_{em}=360 nm) of compound **4** in dichloromethane (c=10^{-5} mol L^{-1}).

The two absorption maxima of compound **5c** are significantly red shifted compared to **4** and are observed at 406 and 339 nm. This red shift is assigned to the extension of the π-conjugation induced by the presence of styryl fragment at the acetyl position of the DHA-difluoroboron complex. However, the introduction of a styryl arm appears to be detrimental for the luminescence properties of the DHA-BF_2 core and only a weak emission centered at 450 nm is now observed upon excitation at 390 nm with a low quantum yield around 0.4%. The replacement of the phenyl ring by a ferrocenyl donor group in **5a** weakly affect the position of these two absorption bands but an additional intense and broad absorption band is observed at 645 nm. This new band is attributed to a *charge-transfer band* (CT band) from the ferrocenyl donor to the DHA-BF_2 acceptor. It should be mentioned that Fc-CHO absorbs at much lower wavelengths. A weak emission at 358 nm was detected with compound **5a** upon excitation at 300 nm. The grafting of a ferrocenyl group does not really affect the luminescence properties the DHA-BF_2-styryl core. Electrochemical or chemical oxidation (with $NOBF_4$) of compound **5a** did not change the luminescence properties. An irreversible extinction of the luminescence was observed upon reduction at −1V versus SCE, likely attributed to the degradation of the compound. With a TTF fragment (**5b**), a CT band is also observed but at higher wavelength (799 nm), which is in line with a stronger donor character compare to a ferrocenyl fragment. Introduction of a styryl arm at the 6 position was also found to be detrimental for the luminescence properties of the DHA-BF_2 core since no emission could have been detected with **3a** and **3c** compounds. It can also be observed that the extension of the π-conjugation, i.e., bathochromic shift of the absorption bands, is much more effective at the acetyl position than in the 6 position. Removal of the BF_2 fragment (compounds **2** and **6**) leads to a blue shift of the absorption bands. This behavior is likely attributed to a decrease of the rigidity and planarity between the DHA fragment and the carbonyl group. The same observation can also be made within the hydrazine series. The absorption spectra of **8c**, the DHA-hydrazone derivative carrying a phenyl ring, displays two strong absorption bands at 365 and 379 nm. **8a** carrying a ferrocene moiety shows the same main absorption peaks at 361 and 376 nm and the expected additional broad CT band due to the presence of the donor fragment on the hydrazone derivative is observed at 483 nm. These two compounds were found to be non-luminescent in solution and in the solid state in contrary to the DHA-azino derivative **9c** carrying a phenyl group and complexed by a BF_2 fragment. The absorption spectra of **9c** displays one main absorption band centered at 358 nm. **9c** is weakly luminescent in dichloromethane solution (ϕ=0.2%) but interestingly it was found that this compound is highly luminescent in the solid state. Upon excitation at 360 nm, this compound shows a strong emission from 410 to 700 nm with a maximum centered at 469 nm (Fig. 5). The solid state quantum yield measured with an integration sphere was found to be around 24%, which is 120 times higher than in solution. The luminescence properties of **9c** appear to be highly sensitive to the aggregation state and in the solid state a strong increase of the luminescence intensity is observed. This phenomenon can be described as an Aggregation Induced Enhancement Emission (AIEE) due to a restricted intramolecular motion[17] or to *J* stacking.[18] More interestingly, the colorimetric coordinate of the emitted light in the CIE diagram were found to be x=0.200 and y=0.314, which is close to white light (x=0.33 and y=0.33).

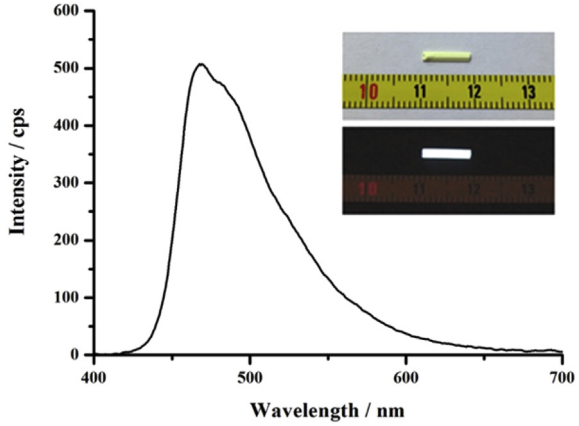

Fig. 5. Solid state emission of compound **9c** under excitation at 360 nm (inset: Photographs of a crystal of compound **9c** under day light (top) and 254 nm UV light (bottom)).

3. Conclusion

In conclusion, we prepared three types of DHA and DHA-BF_2 functionalized at different position by a benzene ring or an electroactive molecule (TTF or Fc). It is worth noting that the molecules where an azino linker is used to connect the DHA to the electrophore are more stable than those involving an ethylenic spacer group especially in the case of the boron difluoride complexes. Indeed, dioxaborine cycles can be easily hydrolyzed leading to the decomplexation while the enaminoketonato boron is more stable. The photophysical behavior of some of these difluoroboron complexes have been investigated. The DHA-BF_2 was found highly luminescent in solution and we observed that substitution of this skeleton induces a significant decrease of the emission properties. Nevertheless, the most interesting derivative is the one where a phenyl ring is linked by an azino spacer group to the DHA-BF_2 moiety. Indeed even if in solution this compound is weakly luminescent, in the solid state a strong increase of the luminescence is observed. Moreover, the colorimetric coordinate of the light emitted let us infer that a fine tuning of the substituent on this skeleton would allowed us to reach the white light.

4. Experimental section

4.1. General

^{1}H NMR, ^{13}C NMR, ^{11}B NMR and ^{19}F NMR spectra were recorded on a Bruker Avance 300 III spectrometer using $CDCl_3$ as solvent unless otherwise stated. Chemical shifts are reported in parts per million. Mass spectra and elemental analysis results were performed by the Centre Régional de Mesures Physiques de l'Ouest (CRMPO), Rennes. Melting points were measured using a Kofler hot stage apparatus and are uncorrected. Cyclic voltammetry were carried out on a 10^{-3} M solution of the compounds in dichloromethane, containing 0.1 M n-Bu_4NPF_6 as supporting electrolyte. Voltammograms were recorded at 100 mV s^{-1} on a platinum disk electrode (1 mm^2). The potentials were measured versus Saturated Calomel Electrode. Compounds **1**,[10] **2c**,[10] **4**[12] and **7**[13] were synthesized according to literature procedure. All the reagents were purchased and used without additional purification. UV–vis spectra were recorded using a Cary 100 UV–vis spectrophotometer (Varian) and CH_2Cl_2 as solvent. Photoluminescence spectra in solution were recorded with a Jobin-Yvon spectrofluorimeter. Quantum yields in solution (ϕsol) were calculated relative to quinine sulfate (ϕ_{ref}=0.546 in H_2SO_4 1N). ϕsol was determined according to the following equation,

$$\phi sol = \phi ref \times 100 \times [(T_s \times A_r)/(T_r \times A_s)] \times [(n_s/n_r)^2]$$

where, subscripts s and r refer, respectively to the sample and reference. The integrated area of the emission peak in arbitrary units is given as *T*, *n* is the refracting index of the solvent (n=1.333 for H_2O and n=1.424 for dichloromethane) and A is the absorbance. Absolute quantum yield and CIE coordinates were measured with a Hamamatsu C9920-03G system.

4.2. Synthesis and characterization

*General procedure for the synthesis of **2a**, **b**.* To a solution of phosphonium salt **1** (0.75 mmol, 382 mg) in 10 mL of dry DMF at 0 °C was slowly added 1.5 mL (1.5 mmol) of freshly prepared 1 M sodium methanolate solution under inert atmosphere. The reaction was kept at room temperature for 1/2 h and ferrocenecarboxaldehyde (0.7 mmol, 150 mg) or Me_3TTFcarboxaldehyde (0.7 mmol, 192 mg) in dry DMF (10 mL) was slowly added. The solution was left overnight under stirring. The medium was acidified with 1 M HCl solution (0.8 mL, 0.8 mmol) and DMF was evaporated. The resulting solid was extracted with CH_2Cl_2 and washed with water and subjected to column chromatography on silica gel with CH_2Cl_2/PE (3/1) as eluent.

2a (56 mg) was obtained as a deep purple solid in 22% yield; mp 172–174 °C; ^{1}H NMR ($CDCl_3$, 300 MHz) δ (ppm) 2.70 (s, 3H, CH_3), 4.20 (s, 5H, Cp), 4.52 (m, 2H, Cp), 4.62 (m, 2H, Cp), 5.93 (s, 1H,=CH), 6.21 (d, 1H, *J*=15 Hz,=CH), 7.59 (d, 1H, *J*=15 Hz,=CH), 16.63 (s, 1H, OH); ^{13}C NMR ($CDCl_3$, 75 MHz) δ (ppm) 30.3, 68.7, 70.0, 71.7, 79.3, 99.2, 100.1, 114.8, 142.32, 161.1, 164.1, 180.8, 204.7; UV–vis λ (ε)= 387 nm (20,800), 534 nm (5500); IR (cm^{-1}) ν=1712, 1610, 1545; HRMS calcd for M^+ ($C_{19}H_{16}O_4{}^{56}Fe$): 364.0398, found: 364.0399.

2b (169 mg) was obtained as a deep purple solid in 57% yield; mp>250 °C (decomp.); ^{1}H NMR ($CDCl_3$, 300 MHz) δ (ppm) 1.96 (s, 6H, CH_3), 2.26 (s, 3H, CH_3), 2.68 (s, 3H, CH_3), 5.80 (d, 1H, *J*=15 Hz,=CH); 5.98 (s, 1H,=CH), 7.36 (d, 1H, *J*=15 Hz,=CH), 16.61 (s, 1H, OH); UV–vis λ (ε)=292 nm (17,000), 330 nm (18,000), 378 nm (32,000), 567 nm (10,000); IR (cm^{-1}) ν=1703, 1593, 1542, 1519; HRMS calcd for $M^{+\cdot}$ ($C_{18}H_{16}O_4S_4$): 423.9931, found: 423.9926.

*General procedure for the synthesis of **3a–c**.* To a solution of **2** (0.25 mmol, 91 mg of **2a**, 106 mg of **2b**, 64 mg of **2c**) in toluene (5 mL) was added dropwise at room temperature and under inert atmosphere 63 μL of boron trifluoride etherate (0.5 mmol). A black solid precipitated immediately, which was filtered under vacuum, washed with toluene and dried. For **3c**, the reaction was refluxed 1 h and the yellow precipitate was filtrated under vacuum, washed with toluene and dried.

3a (98 mg) was obtained as a deep green solid in 95% yield; mp>250 °C (decomp.); ^{1}H NMR ($CDCl_3$, 300 MHz) δ (ppm) 2.84 (s, 3H, CH_3), 4.23 (s, 5H, Cp), 4.64 (m, 2H, Cp), 4.69 (m, 2H, Cp), 6.04 (s, 1H,=CH), 6.27 (d, 1H, *J*=15 Hz,=CH), 7.84 (d, 1H, *J*=15 Hz,=CH); ^{13}C NMR ($CDCl_3$, 75 MHz) δ (ppm) 26.5, 69.9, 70.8, 73.6, 77.3, 99.2, 107.5, 113.9, 148.4, 158.7, 168.6, 178.0, 197.7; ^{11}B NMR ($CDCl_3$, 96 MHz) δ (ppm) −0.03; ^{19}F NMR ($CDCl_3$, 282 MHz) δ (ppm) −141.3; UV–vis λ (ε)=307 nm (1800), 420 nm (11,000), 606 nm (3500); IR (cm^{-1}) ν=1749, 1580, 1496; HRMS calcd for M^+ ($C_{19}H_{15}O_4{}^{11}BF_2{}^{56}Fe$): 412.0381, found: 412.0380.

3b (111 mg) was obtained as a deep purple solid in 94% yield; mp=220 °C (decomp.); ^{1}H NMR (CD_3CN, 300 MHz) δ (ppm) 2.31 (s, 3H, CH_3), 2.65 (s, 6H, CH_3), 2.79 (s, 3H, CH_3), 6.22 (d, 1H, *J*=15 Hz,=CH), 6.49 (s, 1H,=CH), 7.60 (d, 1H, *J*=15 Hz,=CH). ^{11}B NMR ($CDCl_3$, 96 MHz) δ (ppm) −0.99; ^{19}F NMR ($CDCl_3$, 282 MHz) δ (ppm) −150.6; UV–vis λ (ε)=385 nm (16,900), 410 nm (16,200), 636 nm (7500); IR (cm^{-1}) ν=1740, 1620, 1458; HRMS calcd for M^+ ($C_{18}H_{15}O_4{}^{11}BF_2S_4$): 471.9914, found: 471.9924.

3c (70 mg) was obtained after precipitation in CH_2Cl_2 as yellow crystals in 92% yield; mp 240 °C (decomp.); ^{1}H NMR ($CDCl_3$, 300 MHz) δ (ppm) 2.89 (s, 3H, CH_3), 6.22 (s, 1H,=CH), 6.73 (d, 1H, *J*=17 Hz,=CH); 7.42–7.48 (m, 3H, Ar), 7.61 (m, 2H, Ar); 8.83 (d, 1H, *J*=17 Hz,=CH); ^{11}B NMR ($CDCl_3$, 96 MHz) δ (ppm) −0.02; ^{19}F NMR ($CDCl_3$, 282 MHz) δ (ppm) −140.4; UV–vis λ (ε)=395 nm (39,000); IR (cm^{-1}) ν=1756, 1629, 1600, 1509; HRMS calcd for $[M+H]^+$ ($C_{15}H_{12}O_4{}^{11}BF_2$): 305.0791, found: 305.0795.

*General procedure for the synthesis of **5a–c**.* To a hot solution of DHA-BF_2 **4** (216 mg, 1 mmol) in 3 mL of acetic anhydride (60 °C) was added a solution of ferrocenecarboxaldehyde (214 mg, 1 mmol) or a suspension of trimethylTTF-aldehyde (274 mg, 1 mmol) or a solution of benzaldehyde (153 μL, 1.5 mmol) in 2 mL of acetic anhydride. The reaction was heated to 90 °C for 45 min. After cooling, the precipitate was filtered and washed with acetic acid and water.

5a (247 mg) was obtained in 60% yield as a deep green powder; mp 250 °C (decomp.); ^{1}H NMR ($CDCl_3$, 300 MHz) δ (ppm) 2.33 (s, 3H, CH_3), 4.30 (s, 5H, Cp), 4.83 (s, 2H, Cp), 4.93 (s, 2H, Cp), 6.09 (s, 1H,=CH), 7.84 (d, 1H,=CH, *J*=16 Hz), 8.59 (d, 1H,=CH, *J*=16 Hz); ^{13}C NMR ($CDCl_3$, 75 MHz) δ (ppm) 21.1, 71.5, 71.7, 76.1, 79.1, 98.36, 130.1, 114.6, 159.3, 160.6, 171.8, 178.4, 179.8; ^{11}B NMR ($CDCl_3$, 96 MHz) δ (ppm) −0.05; ^{19}F NMR ($CDCl_3$, 282 MHz) δ (ppm) −143.3; UV–vis λ (ε)=330 nm (12,500), 419 nm (57,500), 645 nm (14,500); IR (cm^{-1}) ν=1739, 1632, 1591, 1475; HRMS calcd for M^+ ($C_{19}H_{15}O_4{}^{11}BF_2{}^{56}Fe$); 412.0381, found: 412.0387; Anal. Calcd for $C_{19}H_{15}BF_2FeO_4$: C, 55.39, H, 3.67, found C, 55.65, H, 3.63%.

5b was extracted with CH_2Cl_2 and subjected to column chromatography using first CH_2Cl_2/PE (1/2) and then CH_2Cl_2 as eluent. **5b** (33 mg) was obtained in 7% yield as a green powder; mp>260 °C; ^{1}H NMR ($CDCl_3$, 300 MHz) δ (ppm) 1.97 (s, 3H, CH_3), 1.98 (s, 3H, CH_3), 2.37 (s, 3H, CH_3), 2.41 (s, 3H, CH_3), 6.09 (s, 1H,=CH), 7.42 (d, 1H,=CH, *J*=15 Hz), 8.08 (d, 1H,=CH, *J*=15 Hz); ^{11}B NMR ($CDCl_3$, 96 MHz) δ (ppm) 0.08; ^{19}F NMR ($CDCl_3$, 282 MHz) δ (ppm) −142.6; UV–vis λ (ε)=324 nm (14,000), 432 nm (26,000), 799 nm (78,000); IR (cm^{-1}) ν=2920, 1729, 1641, 1583, 1466, 1402; HRMS calcd for M^+ ($C_{18}H_{15}BF_2O_4S_4$): 471.9909, found: 471.9910.

5c was purified by column chromatography using CH_2Cl_2/PE (4/1) as eluent. **5c** (36 mg) was obtained in 12% yield as a pale yellow powder; mp 254 °C (decomp.); ^{1}H NMR ($CDCl_3$, 300 MHz) δ (ppm) 2.40 (s, 3H, CH_3), 6.16 (s, 1H,=CH), 7.46–7.59 (m, 3H, Ar), 7.78 (m, 2H, Ar), 8.40 (d, 1H,=CH, *J*=15 Hz), 8.46 (d, 1H,=CH, *J*=15 Hz); ^{13}C

NMR ($CDCl_3$, 75 MHz) δ (ppm) 21.4, 103.0, 118.9, 129.2, 129.6, 130.8, 133.7, 134.0, 155.1, 159.0, 174.3, 180.0, 184.8; ^{11}B NMR ($CDCl_3$, 96 MHz) δ (ppm) 0.14; ^{19}F NMR ($CDCl_3$, 282 MHz) δ (ppm) −141.9; UV–vis λ (ε)=339 nm (11,500), 406 nm (40,000); IR (cm^{-1}) ν=2925, 1732, 1631, 1618, 1539, 1501; HRMS calcd for $[M+H]^+$ ($C_{15}H_{12}O_4{}^{11}BF_2$): 305.0791, found: 305.0796.

*General procedure for the synthesis of **6a**, **b**.* To difluoroborane complex **5a** (100 mg, 0.24 mmol) or **5b** (20 mg, 0.042 mmol) was added sodium carbonate (1.0 g, 0.94 mmol) dissolved in a mixture of water (5 mL) and EtOH (5 mL). The medium was refluxed for 2 h. The reaction mixture was cooled and treated with a solution of hydrochloric acid till pH reached 6.5–7. The precipitate that formed was filtered, extracted with CH_2Cl_2, washed with water and dried over magnesium sulfate. The product was purified by column chromatography using CH_2Cl_2/PE (4/1) as eluent.

6a (65 mg) was obtained as a deep purple powder in 75% yield; mp 159–160 °C; ^1H NMR ($CDCl_3$, 300 MHz) δ (ppm) 2.25 (s, 3H, CH_3), 4.20 (s, 5H, Cp), 4.57 (s, 2H, Cp), 4.68 (s, 2H, Cp), 5.92 (s, 1H,=CH), 7.86 (d, 1H,=CH, *J*=16 Hz), 7.99 (d, 1H,=CH, *J*=16 Hz); ^{13}C NMR ($CDCl_3$, 75 MHz) δ (ppm) 20.6, 69.9, 70.1, 72.4, 79.0, 98.9, 102.9, 119.3, 150.0, 161.4, 167.8, 183.7, 190.9; UV–vis λ (ε)=365 nm (32,500), 550 nm (7500); IR (cm^{-1}) ν=1716, 1652, 1609, 1504; HRMS calcd for M^+ ($C_{19}H_{16}O_4{}^{56}Fe$): 364.0398, found: 364.0410.

6b (11 mg) was obtained as a deep blue powder in 64% yield; mp>250 °C; ^1H NMR ($CDCl_3$, 300 MHz) δ (ppm) 1.95 (s, 3H, CH_3), 1.96 (s, 3H, CH_3), 2.27 (s, 6H, CH_3), 5.93 (s, 1H,=CH), 7.46 (d, 1H,=CH, *J*=15 Hz), 7.73 (d, 1H,=CH, *J*=15 Hz), 17.89 (s, 1H, OH); ^{13}C NMR ($CDCl_3$, 75 MHz) δ (ppm) 13.8, 14.8, 20.8, 99.6, 102.5, 113.1, 122.7, 123.4, 124.0, 128.9, 129.6, 133.1, 144.8, 161.1, 168.7, 183.1, 192.0; UV–vis λ (ε)=368 nm (32,600), 600 nm (8200); IR (KBr, cm^{-1}) ν=2921, 1716, 1638, 1618, 1509; HRMS calcd for M^+ ($C_{18}H_{16}O_4S_4$): 423.9926, found: 423.9930.

*General procedure for the synthesis of **8a**, **b**.* To a solution of DHA-hydrazone **7** (182 mg, 1 mmol) in THF (15 mL) was added ferrocenecarboxaldehyde (214 mg, 1 mmol) or Me_3TTFcarboxaldehyde (274 mg, 1 mmol) and 2 mL of HCl 2 M. The reaction mixture was refluxed 2 h. The solvent was removed under vacuum, the solid was extracted with CH_2Cl_2, washed with water and dried over $MgSO_4$.

8 was purified by column chromatography using CH_2Cl_2 as eluent to afford a red solid in 74% yield (280 mg); mp 154 °C; ^1H NMR ($CDCl_3$, 300 MHz) δ (ppm) 2.16 (s, 3H, CH_3), 2.89 (s, 3H, CH_3), 4.23 (s, 5H, Cp), 4.53 (s, 2H, Cp), 4.69 (s, 2H, Cp), 5.75 (s, 1H,=CH), 8.20 (s, 1H,=CH), 16.71 (s, 1H, OH); ^{13}C NMR ($CDCl_3$, 75 MHz) δ (ppm) 17.2, 20.0, 68.8, 69.6, 71.8, 76.5, 95.6, 107.2, 156.4, 163.2, 163.5, 170.9, 184.5; UV–vis λ (ε)=248 nm (86,000), 361 nm (133,000), 376 nm (122,000), 483 nm (22,000); IR (cm^{-1}) ν=1707, 1659, 1600, 1562; HRMS calcd for M^+ ($C_{19}H_{18}N_2O_3{}^{56}Fe$): 378.0667, found: 378.0672. Anal. Calcd for $C_{19}H_{18}FeN_2O_3$: C, 60.34, H, 4.80, N, 7.41, found C, 60.04, H, 4.73, N, 7.10%.

8b was purified by column chromatography using CH_2Cl_2/MeOH (9.8/0.2) as eluent to afford a deep purple powder in 53% yield (232 mg); mp 274 °C; ^1H NMR ($CDCl_3$, 300 MHz) δ (ppm) 1.96 (s, 6H, CH_3), 2.17 (s, 3H, CH_3), 2.26 (s, 3H, CH_3), 2.88 (s, 3H, CH_3), 5.74 (s, 1H, CH), 8.09 (s, 1H, CH=N); ^{13}C NMR ($CDCl_3$, 75 MHz) δ (ppm) 12.7, 12.7, 13.4, 16.0, 18.9, 95.1, 105.8, 112.1, 121.7, 122.1, 142.6, 142.8, 142.9, 162.0, 162.7, 171.6, 183.6; UV–vis λ (ε) 369 nm (34,400), 383 nm (36,300), 525 nm (6600); IR (cm^{-1}) ν=1616, 1590; HRMS calcd for M^+ ($C_{18}H_{18}N_2O_3S_4$) 438.0200, found 438.0194.

*Synthesis of **8c**.* To a solution of DHA-hydrazone **7** (546 mg, 3 mmol) in absolute EtOH (15 mL) was added benzaldehyde (0.3 mL, 3 mmol). The reaction mixture was refluxed for 3 h. The solvent was removed under vacuum and the solid was subjected to column chromatography using CH_2Cl_2/PE (4/1) as eluent to afford **8c** (608 mg) in 75% yield as a pale yellow powder; mp 199 °C; ^1H NMR ($CDCl_3$, 300 MHz) δ (ppm) 2.17 (s, 3H, CH_3), 3.00 (s, 3H, CH_3), 5.76 (s, 1H,=CH), 7.43–7.52 (m, 3H, Ar), 7.66 (d, 2H, *J*=8 Hz, Ar); 8.29 (s, 1H, N=CH); ^{13}C NMR ($CDCl_3$, 75 MHz) δ (ppm) 17.1, 19.9, 96.0, 107.0, 128.3, 129.0, 131.8, 132.7, 154.3, 163.1, 163.5, 172.9, 184.6; UV–vis λ (ε)=365 nm (39,000), 379 nm (35,000); IR (cm^{-1}) ν=2958, 2923, 1702, 1656, 1608, 1574, 1553; HRMS calcd for $[M+Na]^+$ $C_{15}H_{14}N_2O_3Na$: 293.0902, found: 293.0904; Anal. Calcd for $C_{15}H_{14}N_2O_3$: C, 66.66, H, 5.22, N, 10.36; found C, 66.59, H, 5.10, N, 10.31%.

*General procedure for the synthesis of **9a–c**.* An excess of $Et_2O{\cdot}BF_3$ (0.63 mL, 5 mmol) was added to a solution of **8a** (189 mg, 0.5 mmol) or **8b** (220 mg, 0.5 mmol) **8c** (135 mg, 0.5 mmol) containing dry NEt_3 (0.21 mL, 1.5 mmol) in 15 mL of dry and degassed CH_2Cl_2 under inert atmosphere. The reaction mixture was stirred at room temperature for 12 h. The organic phase was washed with water and dried over $MgSO_4$ and subjected to column chromatography using CH_2Cl_2 as eluent.

9a (164 mg) was obtained as a red solid in 77% yield; mp 206 °C; ^1H NMR ($CDCl_3$, 300 MHz) δ (ppm) 2.31 (s, 3H, CH_3), 2.81 (s, 3H, CH_3), 4.32 (s, 5H, Cp), 4.58 (t, 2H, *J*=2 Hz, Cp), 4.76 (s, 2H, *J*=2 Hz, Cp), 6.07 (s, 1H,=CH), 8.63 (s, 1H,=CH); ^{13}C NMR ($CDCl_3$, 75 MHz) δ (ppm) 17.9, 20.6, 69.4, 70.0, 72.5, 77.2, 96.7, 102.4, 160.5, 164.8, 167.6, 168.8, 172.3; ^{11}B NMR ($CDCl_3$, 96 MHz) δ (ppm) −19.39; ^{19}F NMR ($CDCl_3$, 282 MHz) δ (ppm) −136.6; UV–vis λ (ε)=289 nm (45,000), 353 nm (111,000), 500 nm (19,000); IR (cm^{-1}) ν=1712, 1650, 1609, 1562, 1506; HRMS calcd for M^+ ($C_{19}H_{17}N_2O_3{}^{11}BF_2{}^{56}Fe$): 426.0650, found: 426.0660.

9b (56 mg) was obtained as a red solid in 23% yield; mp>260 °C; ^1H NMR ($CDCl_3$, 300 MHz) δ (ppm) 1.96 (s, 6H, CH_3), 2.33 (s, 3H, CH_3), 2.92 (s, 3H, CH_3), 6.06 (s, 1H,=CH), 8.65 (s, 1H,=CH); ^{11}B NMR ($CDCl_3$, 96 MHz) δ (ppm) −0.14; ^{19}F NMR ($CDCl_3$, 282 MHz) δ (ppm) −136.4; UV–vis λ (ε)=369 nm (34,000), 558 nm (6700); HRMS calcd for M^+ ($C_{18}H_{17}N_2O_3{}^{11}BF_2$): 486.01832, found: 486.0184.

9c (95 mg) was obtained as a yellow solid in 60% yield; mp 202 °C; ^1H NMR ($CDCl_3$, 300 MHz) δ (ppm) 2.34 (s, 3H, CH_3), 2.96 (s, 3H, CH_3), 6.08 (s, 1H,=CH), 7.45–7.57 (m, 3H, Ar), 7.86 (d, 2H, *J*=6 Hz, Ar); 8.78 (s, 1H,=CH); ^{13}C NMR ($CDCl_3$, 75 MHz) δ (ppm) 18.2, 20.7, 96.9, 102.4, 129.1, 129.2, 132.8, 132.9, 160.4, 162.4, 169.7, 170.4, 173.0; ^{11}B NMR ($CDCl_3$, 96 MHz) δ (ppm) −0.07; ^{19}F NMR ($CDCl_3$, 282 MHz) δ −136.6; UV–vis λ (ε)=358 nm (26,500); IR (cm^{-1}) ν=1731, 1637, 1510, 1449; HRMS calcd for $[M+Na]^+$ $C_{15}H_{13}N_2O_3{}^{11}BF_2Na$: 341.0885, found: 341.0884.

4.3. Crystallography

Single-crystal diffraction data were collected on APEX II Bruker AXS diffractometer, Mo Kα radiation (λ=0.71073 Å), for compounds **5a**, **5b**, **7**, **8a** and **9a** (Centre de Diffractométrie X, Université de Rennes, France). The structures were solved by direct methods using the SIR97 program,[19] and then refined with full-matrix least-square methods based on F2 (SHELX-97)[20] with the aid of the WINGX program.[21] All non-hydrogen atoms were refined with anisotropic atomic displacement parameters. H atoms were finally included in their calculated positions.

Crystal data for **5a**: ($C_{19}H_{15}BF_2FeO_4$); *M*=411.97. *T*=294 (2) K; monoclinic P $2_1/c$, *a*=11.323 (5), *b*=10.313 (7), *c*=15.246 (9) Å, β=103.71 (3) °, *V*=1729.6 (17) $Å^3$, *Z*=4, *d*=1.582 g cm^{-3}, μ=0.915 mm^{-1}. A final refinement on F^2 with 3903 unique intensities and 245 parameters converged at $\omega R(F^2)$=0.1034 (*R(F)*=0.0429) for 2554 observed reflections with $I>2\sigma(I)$.

Crystal data for **5b**: ($C_{18}H_{15}BF_2O_4S_4$); *M*=472.35. *T*=150 (2) K; monoclinic P $2_1/c$, *a*=14.6844 (17), *b*=12.3494 (15), *c*=11.3986 (10) Å, β=102.523 (4) °, *V*=2017.9 (4) $Å^3$, *Z*=4, *d*=1.555 g cm^{-3},

μ=0.512 mm^{-1}. A final refinement on F^2 with 4584 unique intensities and 266 parameters converged at $\omega R(F^2)$=0.1122 ($R(F)$=0.0523) for 2425 observed reflections with $I>2\sigma(I)$.

Crystal data for **7**: ($C_8H_{10}N_2O_3$); M=182.18 T=100 K; orthorhombic Pcnb, a=7.5868 (5), b=14.5439 (9), c=14.8425 (9) Å, $\alpha=\beta=\gamma$=90.0°, V=1637.75 (18) Å^3, Z=8, d=1.478 g cm^{-3}, μ=0.115 mm^{-1}. A final refinement on F^2 with 1870 unique intensities and 126 parameters converged at $\omega R(F^2)$=0.1255 ($R(F)$=0.0459) for 1520 observed reflections with $I>2\sigma(I)$.

Crystal data for **8a**: ($C_{19}H_{18}FeN_2O_3$); M=378.2. T=150 (2) K; monoclinic P $2_1/c$, a=7.4264 (3), b=18.3887 (8), c=12.2869 (5) Å, β=103.5250 (10)°, V=1631.39 (12) Å^3, Z=4, d=1.54 g cm^{-3}, μ=0.946 mm^{-1}. A final refinement on F^2 with 3735 unique intensities and 231 parameters converged at $\omega R(F^2)$=0.0642 ($R(F)$=0.0258) for 3309 observed reflections with $I>2\sigma(I)$.

Crystal data for **9a**: ($C_{19}H_{17}BF_2FeN_2O_3$); M=426.01. T=150 (2) K; monoclinic P 1 $2_1/n$, a=7.0024 (12), b=13.757 (2), c=18.610 (3) Å, β=90.130 (8)°, V=1792.7 (5) Å^3, Z=4, d=1.578 g cm^{-3}, μ=0.885 mm^{-1}. A final refinement on F^2 with 4072 unique intensities and 256 parameters converged at $\omega R(F^2)$=0.0953 ($R(F)$=0.0477) for 2797 observed reflections with $I>2\sigma(I)$.

Acknowledgements

This work was supported by the PHC Tassili 11 MDU 828.

Supplementary data

Crystallographic data for structural analysis have been deposited with the Cambridge Crystallographic Data Centre, CCDC No 1428516–1428520 for compounds **5a**, **5b**, **7**, **8a** and **9a,** respectively. Copies of this information may be obtained free of charge from The CCDC, 12 Union Rd, Cambridge CB2 1EZ, UK (fax: +44 1223 336033; e-mail: deposit@ccdc.cam.ac.uk or http://www.ccdc.cam.ac.uk).

Supplementary data associated with this article can be found in the online version, at http://dx.doi.org/10.1016/j.tet.2015.11.034.

References and notes

1. Gupta, G. K.; Mittal, A.; Kumar, V. *Lett. Org. Chem.* **2014**, *11*, 273–286.
2. Lorcy, D.; Bellec, N.; Fourmigué, M.; Avarvari, N. *Coord. Chem. Rev.* **2009**, *253*, 1398–1438.
3. (a) Casabó, J.; Marquet, J.; Moreno-Mañas, M.; Prior, M.; Teixidor, F.; Florencio, F.; Martínez-Carrera, S.; García-Blanco, S. *Polyhedron* **1987**, *6*, 1235–1238; (b) Luo, H.; Liu, S.; Rettig, S. J.; Orvig, C. *Can. J. Chem.* **1995**, *73*, 2272–2281; (c) Chalaça, M. Z.; Figueroa-Villar, J. D.; Ellena, J. A.; Castellano, E. E. *Inorg. Chim. Acta* **2002**, *328*, 45–52; (d) Cindrić, M.; Vrdoljak, V.; Strukan, N.; Tepeš, P.; Novak, P.; Brbot-Saranović, A.; Giester, G.; Kamenar, B. *Eur. J. Inorg. Chem.* **2002**, 2128–2137; (e) Hsieh, W.-Y.; Zaleski, C. M.; Pecoraro, V. L.; Fanwick, P. E.; Liu, S. *Inorg. Chim. Acta* **2006**, *359*, 228–236; (f) Chitrapriya, N.; Mahalingam, V.; Zeller, M.; Jayabalan, R.; Swaminathan, K.; Natarajan, K. *Polyhedron* **2008**, *27*, 939–946; (g) Djedouani, A.; Boufas, S.; Bendaas, A.; Allain, M.; Bouet, G. *Acta Cryst.* **2009**, *E65*, m1205–m1206.
4. (a) Gupta, A. K.; Pal, R. *World J. Pharm. Pharm. Sci.* **2015**, *4*, 386–425; (b) Gupta, A. K.; Pal, R.; Beniwal, V. *World J. Pharm. Pharm. Sci.* **2015**, *4*, 990–1008.
5. Xia, M.; Wu, B.; Xiang, G. *J. Fluor. Chem.* **2008**, *129*, 402–408.
6. (a) Pellon, P.; Brulé, E.; Bellec, N.; Chamontin, K.; Lorcy, D. *J. Chem. Soc. Perkin Trans. 1* **2000**, 4409–4412; (b) Bellec, N.; Lorcy, D. *Tetrahedron Lett.* **2001**, *42*, 3189–3191; (c) Pellon, P.; Gachot, G.; Le Bris, J.; Marchin, S.; Carlier, R.; Lorcy, D. *Inorg. Chem.* **2003**, *42*, 2056–2060; (d) Massue, J.; Bellec, N.; Chopin, S.; Levillain, E.; Roisnel, T.; Clérac, R.; Lorcy, D. *Inorg. Chem.* **2005**, *44*, 8740–8748; (e) Gachot, G.; Pellon, P.; Roisnel, T.; Lorcy, D. *Eur. J. Inorg. Chem.* **2006**, 2604–2611; (f) Bellec, N.; Massue, J.; Roisnel, T.; Lorcy, D. *Inorg. Chem. Commun.* **2007**, *10*, 1172–1176; (g) Guerro, M.; Pham, N. H. P.; Massue, J.; Bellec, N.; Lorcy, D. *Tetrahedron* **2008**, *64*, 5285–5290; (h) Gachot, G.; Pellon, P.; Roisnel, T.; Lorcy, D. *J. Organomet. Chem.* **2009**, *694*, 2531–2535; (i) Bakhta, S.; Guerro, M.; Kolli, B.; Barrière, F.; Roisnel, T.; Lorcy, D. *Tetrahedron Lett.* **2010**, *51*, 4497–4500; (j) Huang, K. L.; Bellec, N.; Guerro, M.; Camerel, F.; Roisnel, T.; Lorcy, D. *Tetrahedron* **2011**, *67*, 8740–8746.
7. Batail, P. Ed. *Chem. Rev.* **2004**, *104*, 4887–5781.
8. van Staveren, D. R.; Metzler-Nolte, N. *Chem. Rev.* **2004**, *104*, 5931–5985.
9. Guerro, M.; Dam, T. U.; Bakhta, S.; Kolli, B.; Roisnel, T.; Lorcy, D. *Tetrahedron* **2011**, *67*, 3427–3433.
10. Bacardit, R.; Moreno-Mañas, M.; Pleixats, R. *J. Heterocycl. Chem.* **1982**, *19*, 157–160.
11. Bartle, K. D.; Edwards, R. L.; Jones, D. W.; Mir, I. *J. Chem. Soc. C* **1967**, 413–419.
12. (a) Manaev, A. V.; Tombov, K. V.; Traven, V. F. *Russ. J. Org. Chem.* **2008**, *44*, 1054–1060; (b) Ramkumar, K.; Tombov, K. V.; Gundla, R.; Manaev, A. V.; Yarovenko, V.; Traven, V. F.; Neamati, N. *Bioorg. Med. Chem.* **2008**, *16*, 8988–8998.
13. (a) Mahesh, V. K.; Gupta, R. S. *Indian J. Chem.* **1974**, *12*, 570–572; (b) Djerrari, B.; Essassi, E.; Fifani, J. *Bull. Soc. Chim. Fr.* **1991**, 521–524.
14. Amar, A.; Meghezzi, H.; Boucekkine, A.; Kaoua, R.; Kolli, B. *C. R. Chim.* **2010**, *13*, 553–560.
15. Guerro, M.; Roisnel, T.; Lorcy, D. *Tetrahedron* **2009**, *65*, 6123–6127.
16. Olmsted, J. *J. Phys. Chem.* **1979**, *83*, 2581–2584.
17. Mei, J.; Hong, Y.; Lam, J. W. Y.; Qin, A.; Tang, Y.; Tang, B. Z. *Adv. Mater.* **2014**, *26*, 5429–5479.
18. (a) Wang, S.; Xue, P.; Wang, P.; Yao, B. *New J. Chem.* **2015**, *39*, 6874–6881; (b) Würthner, F.; Kaiser, T. E.; Saha-Möller, C. R. *Angew. Chem., Int. Ed.* **2011**, *50*, 3376–3410.
19. Altomare, A.; Burla, M. C.; Camalli, M.; Cascarano, G.; Giacovazzo, C.; Guagliardi, A.; Moliterni, A. G. G.; Polidori, G.; Spagna, R. *J. Appl. Crystallogr.* **1999**, *32*, 115–119.
20. Sheldrick, G. M. *Acta Crystallogr.* **2008**, *A64*, 112–122.
21. Farrugia, L. J. *J. Appl. Crystallogr.* **1999**, *32*, 837–838.